OPEN ACCESS



Prevalence of Extra Power-Law Spectral Components in Short Gamma-Ray Bursts

Qing-Wen Tango, Kai Wang, Liang Lio, and Ruo-Yu Liu, 50

¹ Department of PhysicSchool of ScienceNanchang UniversityNanchang 330031People's Republic of China; qwtang@ncu.edu.cn ² Department of Astronomy, School of Physics, Huazhong University of Science and Technology, Wuhan 430074, People's Republic of China; kaiwang@hust.edu

3 ICRANet, Piazza della Repubblica 10,65122 Pescaraṭaly

⁴ School of Astronomy and Space Science anjing University Xianlin Road 163, Nanjing 210023 People's Republic of China; ryliu@nju.edu.cn ⁵ Key Laboratory of Modern Astronomy and Astrophysics (Nanjing University) inistry of Education, Nanjing 210023, People's Republic of China Received 2021 March 2; revised 2021 September 9; accepted 2021 September 13; published 2021 December 6

A prompt extra power-law (PL) spectral component that usually dominates the spectral energy distribution below tens of keV or above ~10 MeV has been discovered in some brightnma-ray bursts (GRBIs)owever its origin is still unclear. In this paper, we present systematican alysis of 13 Fermi short GRBs, as of 2020 August, with contemporaneous keV-MeV and GeV detections during the prompt emission phase. We find that the extra PL component is a ubiquitous spectral feature for short GRBs, showing up in all 13 analyzed GRBs. The PL indices are mostly harder than -2.0, which may be well reproduced by considering the electromagnetic cascade induced by ultrarelativistic protons or electrons accelerated in the prompt emission phase. The average flux of these extra PL components positively correlat with that of the main spectral components, which implies they may share the same physical origin.

Unified Astronomy Thesaurus concepts: Gamma-ray bursts (629); High energy astrophysics (739); Astronomy data analysis (1858)

1. Introduction

the universe. They can be divided into two phenomenological categories based on their duration in the prophatsenamely, 2 s. Various physical models have been proposed to explain the SGRBs. In previous studies, only two SGRBs, namely, prompt emission, such as the photospheriomodel (Rees & Mészáros 2005; Giannios & Spruit 2007; Pe'er 2008; Beloborodov extra PL componentn the spectrum (Ackermann et 2010; 2011), the internal shock model (Rees & Mészáros 1994; Kobayashet al. 1997; Daigne & Mochkovitch 1998) and the magneticreconnection mode(Spruit et al. 2001; Zhang & radiation mechanism and can help us to understandtheir underlying physicalprocessesObservationallyGRB prompt emission exhibits diverse spectral properties. Those spectra in the keV-MeV energy range can generally be fitted by some empirical The physicabrigin of the extra PL spectratomponents has functions such as the Band function (BAND component) (Band dissipation models (Assert of the Component) of the Indian Police of the Indian Pol with a high-energy exponential cutoff function (CPL component), 12 2010a; Asano & Mészáros 2011; Arimoto e£8£0) and et al. 1993), a simple power-law function (PL component?) L board Fermi (Poolakkil et al. 2021), hereafter the GBM catalog.

spectra of some GRBs consist of more than one component, example a BAND component with a PL component for GRB 080916C, GRB 090510, GRB 0909026A, and GRB 110731A (Ryde et al. 2010; Ackermann et al. 2010, 2013); a CPL component with a PL component for GRB 090902B (time-onentat GeV band. Aside from the hadronic origin model he

Original content from this work may be used under the terms of the Creative Commons Attribution 4.0 licence. Any further distribution of this work must maintain attribution to the author(s) and the title of the work, journal citation and DOI.

resolved),110920A,GRB 160107A,and GRB 160709A (Basak Gamma-ray bursts (GRBs) are the most energetic explosions in Rao 2013; Ryde et al. 2010; lyyani et al. 2015; Kawakubo et al. 2018; Tak et al. 2019).

There are 186 GRBs reported in the 10 yr catalog (hereafter long GRBs (LGRBs) and short GRBs (SGRBs), separated at about August, among which 169 are LGRBs and 17 are Tak et al. 2019). In order to further search for and explore the properties of the extra PL component, here we perform a Yan 2011). Spectral analysis is thus the key to investigate the GRB capacitation mechanism and capable us to understand their range detected between 2008 August and 2020 August. The same dissipation models (Asano et al. 2009; Bošnjak et al. 2009; Corsi and a smoothly broken PL function (SBPL component), based of the sternal special control of the sternal control of Combining these the observations of the Large Area Telescope CDB (AT) (LAT) on board Fermi, it is interesting to note that the keV–GeV ome GRBs (Tang ed. 2017). Even in the internal issipation models it is not clear yetfrom which mechanism the extra PL componentarises. As shown in previous literature, either the photopion production of Bethe-Heitlemair production of relativistic protons can reproduce the additispactrum compintegrated), GRB 100414A, and GRB 160709A (Ackermann et al. 2013; Tak et al. 2019); and a blackbody component (BB or multi-produce such a spectral feature (Wang et al. 2018). Therefore, it BB) with a PL component for GRB 081221, GRB 090902B (time and GeV observation as will also be discussed in this study, observations at lower energies may provide a clue to differentiate these models.

> The rest of the paper is organized as follows. In Section 2 perform the spectral analysis of selected GRBs. In Section 3, the

Table 1 Durations and Positions of 13 GRBs in Our Sample

GRB	GBM T ₀ ^a	GBM T ₉₀	GBM T ₀₅	GBM T ₉₅	LLE Detection	LAT R.A. ^c	LAT Decl. ^c	LAT Ref.d
	(s)	(s)	(s)					
081024B	246576161.864	0.640	-0.064	0.576	Yes	323.01	20.84	(1)
081102B	247308301.506	1.728	-0.064	1.664	L	212.95	30.33	Ĺ
090227B	257452263.407	0.304	-0.016	0.288	Yes	11.80	32.20	L
090228A	257489602.911	0.448	0	0.448	L	98.60	-28.79	L
090510	263607781.971	0.960	-0.048	0.912	Yes	333.57	-26.62	L
110728A	333508824.816	0.704	-0.128	0.576	L	173.57	4.34	L
120830A	368003226.533	0.896	0	0.896	L	88.59	-28.79	L
120915A	369360044.638	0.576	-0.320	0.256	L	240.95	57.04	L
140402A	418090209.998	0.320	-0.128	0.192	L	207.66	5.97	L
141113A	437559466.503	0.448	-0.064	0.384	L	182.32	77.38	L
171011C	529442792.946	0.480	-0.448	0.032	L	168.48	10.03	L
160709A	489786547.512	0.448	0.320	0.768	Yes	236.11	-28.51	(2)
190515A	579587588.135	1.264	-0.112	1.152	L	137.69	29.28	(3)

Notes.

spectral fitting results are presented and discussed. In Section datwere available in the High Energy Astrophysics Science discuss the possible origin the PL spectralcomponentThe conclusions are presented in Section 5.

2. Methodology

2.1. Sample Selection

during the GBM T₉₀ interval, during which 90% of the burst fluence (50-300 keV) accumulated With a contemporaneous detection by the LAT and the GBM, we thus can perform a broadband spectrahalysis between GBM₀F and GBM T₉₅. which are the start and end of GBMT

Among the 17 shorbursts presented in the LAT cataloge. exclude 5 GRBs with no high-energy photons detected above 100 MeV during the GBM₀Intervals, i.e., GRB 090531B, GRB 110529A,GRB 160829A,GRB 170127Cand GRB 180703B. Moreover,we also exclude GRB 160702A as its GBM data are because ouspectralanalysis is performed fothe GRBs with sample a short burs RB 190515A (Kocevski et 2019), that satisfies ouselection criterion and was detected after LAT catalog time period,namely between 2018 Augustand 2020 August. Finally, we also include the long GRB 160709A, although0227B, GRB 090510, and GRB 160709A. Events with 0.32 to ~0.77 s post-trigger time, as discussed in Tak et al. (2015)

Our sample includes 13 SGRBs from 2008 August to 2020 August, which are listed in Table 1, where the GBM trigger time (T₀ in Mission Elapsed Time, MET), T_{0.5}, and T_{0.5} are reported. Positions reported by the LAT catalog are employed for the LAT data reduction as shown in Table 1.

2.2. Event Selection and Background Estimation

Fermi-GBM and Fermi-LAT data are used in our spectral analysis. For four GRBs shown in Table 1, Fermi-LAT Low-Energy (LLE) data are also combined in the spectral fitting. All ⁶

Archive Research Center.

GBM data. For each GRB, we select the three NaI detectors closest to the GRB position and one BGO detector with the lowest angle of incidence, which are presented in Table 2. We analyze Na time-tagged event (TTE) data with energy between 8 and 900 keV as well as BGO TTE data with energy between 250 keV and The main criterion employed to select our sample is that high40 MeV, excluding the overflow channels. The GBM backgrounds

energy photons need to be detected by the Fermi-LAT instrument usually estimated by fitting the observed TTE data tens of seconds before and after the source emission intervals. Because o the short durations (<2 s) in our sample, we found that two time intervals are reasonable to derive a good count-rate background fo the selected GRB detectors through autodetermined polynomial order fitting, such as [-25, -10] and [15, 30] away from the GBM trigger time. Instrumentesponse files are selected with the rsp2 files; however, if no rsp2 files are included in the archived GBM data for some GRBs such as GRB 120830AGRB 120915A, GRB 140402A, and GRB 141113A, the rsp files are selected not archived in the GBM catalog. Furthermore, we include in offelatively short durations (von Kienlin et al. 2014; Narayana Bhat et al. 2016).

LLE data. There are four GRBs in our sample with LLE detection as shown in Table 1such as GRB 081024BGRB both catalogs classify it as a long burst. Indeed, Tak et al. (2019) between 20 and 100 MeV are selected in our spectral consider the main bursting phase of GRB 160709A, ranging from CRM details the same as that of

LAT data. LAT-Transient020E events with a zenith angle cut of 100° are selected for each burst, whose energy are between 100 MeV and 10 Ge\rightarrow or GRB 090510 the highest photon energy is abou80 GeV; thus the maximum energy is 100 GeV. Region of interest (ROI) is chosen within the radius of 12° from the localization report in Table 1.

After the eventselection, the count-rate lightcurve is built for each GRB. For example, the composite light curve for GRB 081024B is shown in Figure 1.

^a GBM burst trigger time in the format of the Fermi Mission Elapsed Time.

b "Yes" indicates that Fermi-LAT Low-Energy (LLE) data are available.

^c Central position employed for the Fermi-LAT detection.

^d (1) Ajello et al. (2019); (2) Tak et al.(2019); (3) Kocevski et al.(2019).

e For GRB 160709A,the selected time range is the main prompt GRB emission phase reported in Tak(@0dl9).

https://fermi.gsfc.nasa.gov/ssc/data/access/

Table 2 Information for the Selected GBM Detectors

GRB name	First Na	D ^a (degree)	Second Na	D ^a (degree)	Third Na	D ^a (degree)	BGO	D ^a (degree)
081024B	n0	30.98	n6	23.56	n9	27.67	b1	73.66
081102B	n0	30.66	n1	18.99	n5	44.20	b0	45.46
090227B	n1	27.27	n2	19.31	n5	51.05	b0	54.22
090228A	n0	10.35	n1	24.73	n3	40.40	b0	67.17
090510	n0	34.17	n6	7.07	n7	32.68	b1	81.59
110728A	n0	31.01	n1	33.34	n9	28.14	b1	87.21
120830A	n0	22.98	n1	21.41	n3	39.17	b0	53.13
120915A	n0	17.40	n3	36.17	n6	28.08	b0	79.00
140402A	n0	28.28	n3	32.60	n6	20.26	b0	84.18
141113A	n3	33.64	n6	38.46	n7	33.70	b1	89.78
160709A	n3	13.06	n4	42.93	n6	44.79	b0	70.29
171011C	n0	25.21	n1	23.77	n3	37.08	b0	51.29
190515A	n0	38.36	n1	43.30	n9	18.98	b1	77.38

Note.

2.3. Fitting Models

In order to test the existence of the additionaPL spectral component, six typical empirical functions are employed as the fitting models to fit the broadband gamma-ray data of each GRB, which are described below:

(i) The blackbody (BB) function, which is usually modified by the Planck spectrum and given by the photon flux

$$\frac{dN}{dE} = A_{BB} \frac{E^2}{\exp[E/kT] - 1},\tag{1}$$

is an output parameter in common. It is found the peak energy law function (CPL+PL), that is in the E2dN dE spectrum of the BB is about 3.92 times the value of kT, that is, E_{p,BB}≈ 3.92kT. In all the functions here and below, A is the normalization constant.

(ii) The Band function (BAND), which is written in the same way as in Band et al.(1993),

$$\frac{dN}{dE} = A_{\text{BAND}}$$

$$\int \left(\frac{E}{100 \text{ keV}}\right)^{a} e^{\left[\frac{E}{2+a}\right]/E_{p}}, \qquad E_{\frac{a-b}{2+a}}E_{p}$$

$$\left\{\left(\frac{(a-b)E_{p}}{(2+a)100 \text{ keV}}\right)^{(a-b)} e^{(b-a)} \left(\frac{E}{100 \text{ keV}}\right)^{b}, \quad E_{\frac{a-b}{2+a}}E_{p}, \quad (2)\right\}$$

photon index respectively and E_p is the peak energy in the E2dN dE spectrumwhich is reported in Section Results as E_{p,BAND} (iii) The cutoff power-law model (CPL)written as

$$\frac{dN}{dE} = A_{\text{CPL}} \left(\frac{E}{100 \text{ keV}} \right)^{a} e^{E/E_c}, \tag{3}$$

where α is the photon index and E is the cutoff energy,the peak energy in the $E^2dN dE$ spectrum for the CPL (E_{CPI}) equals $(2 + \alpha)E$, say, E_p , $CPL = (2 + \alpha)E_c$. (iv) The composite function of the BB and a simple power-

law function (BB+PL), that is,

$$\frac{dN}{dE} = \frac{dN}{dE}\Big|_{BB} + A_{PL} \left(\frac{E}{100 \text{ keV}}\right)^{G_{PL}}, \tag{4}$$

where $\left(\frac{dN}{dE}\right)_{BB}$ is the same as Equation (1) and \overline{I} is the photon index of the PL function.

(v) The composite function of the BAND and a simple power-law function (BAND+PL), that is,

$$\frac{dN}{dE} = \frac{dN}{(dE)}_{BAND} + A_{PL} \left(\frac{E}{100 \text{ keV}}\right)^{G_{PL}}, \tag{5}$$

where $\left(\frac{dN}{dE}\right)_{BAND}$ is the same as Equation (2) and the list the photon index of the PL function.

where k is the Boltzmann's constant, and the joint parameter kT (vi) The composite function of the CPL and a simple power-

$$\frac{dN}{dE} = \frac{dN}{(dE)}_{CPL} + A_{PL} \left(\frac{E}{100 \text{ keV}}\right)^{\zeta_{PL}}, \tag{6}$$

where $\left(\frac{dN}{dE}\right)_{CPL}$ is the same as Equation (3) and Γ_{PL} is the photon index of the PL function.

2.4. Spectral Fitting and the Best-fitting Model Selection

In this work, we use the Markov Chain Monte Carlo (MCMC) fitting technique based on the Bayesian statistic by using the Multi-Mission Maximum Likelihood package (3ML; Vianello et al. 2015) to carry out all spectralanalysesand parameter where α and β are the low-energy photon index and high-energy and the posterior sampling of the parameter space in each fitting model.

2.4.1. Informative Priors Selection

The informative priors are adopted by using the typical spectral parameter from the Fermi-GBM catalog (Poolakkil et al. 2021), hereafterwe call it typical priors (TP). For all parameters in the TP scenario, we set the initial parameter values and the parameter range to be the same as the default value in the 3ML package exceptfor the normalization (A), whose lower bound and uppebound are calculated as 10 and 10 times its initial value, respectively. The distribution of the normalization (A) is the logarithm uniform distribution (LogU), the photon indices $(\alpha, \beta, \text{ and } \Gamma)$ have a Gaussian distribution (G), and parameters in units of kely (E, and kT) are distributed in a logarithm normadistribution (LogN). For

^a Angular separation between the pointing of the GBM detector and the GRB position in a unit of degree

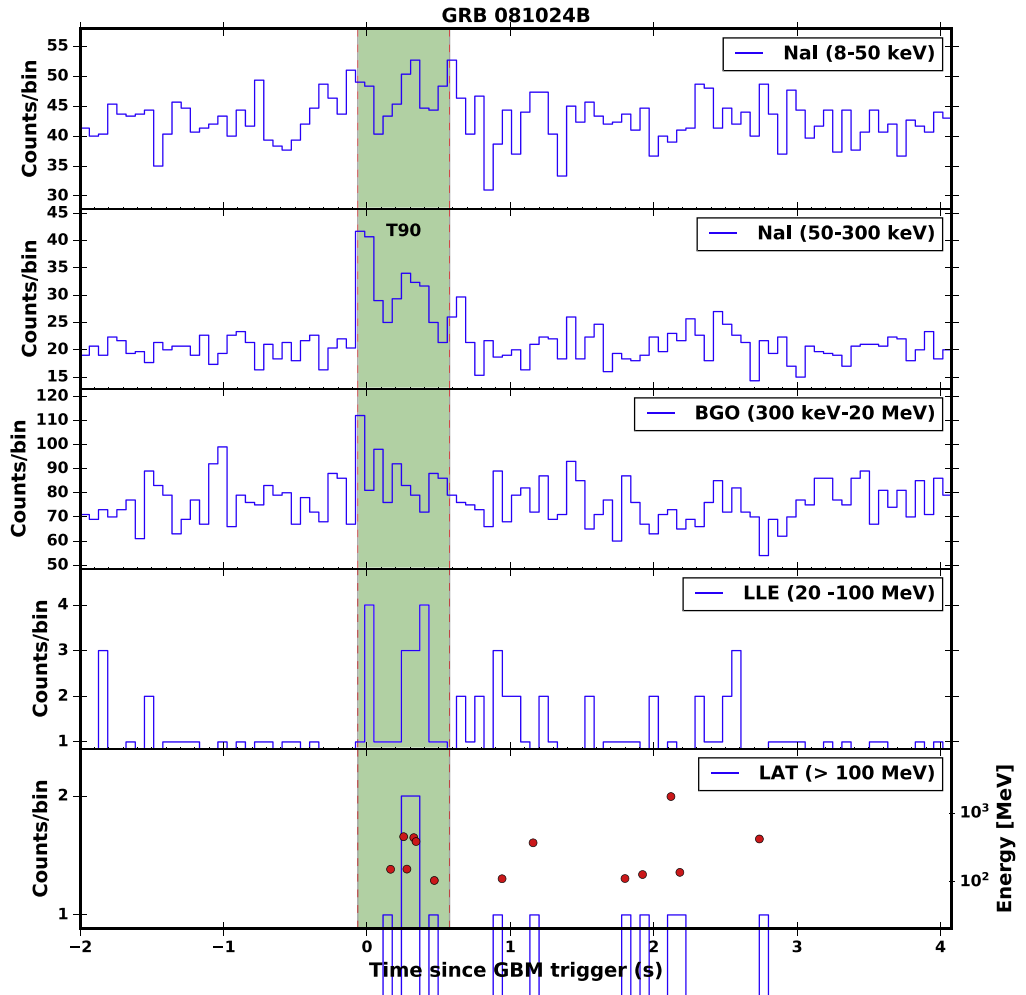


Figure 1. Composite light curve for GRB 081024B. The average count rate of three Nal detectors (the first two panels), BGO (the third panel), LLE (the fourth panel and LAT transient-class events above 100 MeV within a 12° ROI (bottom panel). The shadowed region is the selected time interval to be analyzed. The filled circle are events that have a probability >0.9 of being associated with the GRB.

Table 3 **Prior Setting**

Function	Parameter	Initial Value	Parameter Range	TP Scenarið
PL	Α, Γ	10 ⁻⁴ , -2.0	[10 ⁻⁹ , 10], [-10.0, 10.0]	logU, G
BB	Α, kT	10 ⁻⁴ , 30	[10 ⁻⁹ , 10], [0, 10 ⁵]	logU, LogN
BAND	Α, α, β, Ε _ρ	10 ⁻⁴ , -1.0, -2.0, 500	[10 ⁻⁹ , 10], [-1.5, 3.0], [-5.0, -1.6], [0, 10 ⁷]	logU, G, G, LogN
CPL	Α, α, Ε _c	10 ⁻⁴ , -2.0, 30	[10 ⁻⁹ , 10], [-10.0, 10.0], [0, 10 ⁷]	logU, G, LogN

Note.

all Gaussian distributions (G) the central value (µ) equals the initial parametervalue and the one standard deviation (oi)s fixed at 0.5. For all logarithm normal distributions (logN), both scenario are presented in the following sections. μ and σ are at the initial parameter values. The TP scenario has been used in several publications for the spectral analysis of the Fermi-GBM GRBs (Li2019; Yu et al. 2019; Li et al. 2021).

The details of these priors are presented in Table F.or the composite models (BB+PL,BAND+PL, and CPL+PL), we

parameter ranges are the same as those in the TP scenario butses multiple walkers to explore the parameter space of the with the uniform parameter distributions. Results in the UP scenario are presentedin Appendix A, which draws the

conclusion that the resultant parameters in both scenarios are consistentwith each other; therefore, the results in the TP

2.4.2. Posterior Sampling and the Best-fitting Model Selection

We employ emcess sampling method included in the 3ML packageto sample the posteriowhich is an extensive pureuse the joint informative priors above. We also test the uniformPython implementation of Goodman & Weare's Affine Invariant priors (UP) for all spectral parameters, whose initial values and MCMC Ensemble sampler (Goodman & Weare 2016) incee posterior. For each sampling, we set the number of chains (walkers) to 20; the number of learning samples to 3000, which

^a For the typical priors (TP), LogU represents the logarithm uniform distribution Grepresents the Gaussian distribution and LogN is the logarithm normal

Table 4 ΔBIC and the Best-fitting Models

GRB	BB	BAND	CPL	BB+PL	BAND+PL	CPL+PL	Best Modef
081024B	>10 ^b	>10	>10	0	>10	>10	BB+PL
081102B	>10	>10	>10	0	>10	>10	BB+PL
090227B	>10	>10	>10	>10	>10	0	CPL+PL
090228A	>10	>10	>10	>10	3	0	CPL+PL
090510	>10	>10	>10	>10	0	>10	BAND+PL
110728A	>10	>10	>10	0	>10	>10	BB+PL
120830A	>10	>10	>10	>10	>10	0	CPL+PL
120915A	>10	>10	>10	0	>10	>10	BB+PL
140402A	>10	>10	>10	0	>10	>10	BB+PL
141113A	>10	>10	>10	0	>10	>10	BB+PL
160709A	>10	>10	>10	>10	3	0	CPL+PL
171011C	>10	>10	>10	0	>10	>10	BB+PL
190515A	>10	>10	>10	0	>10	>10	BB+PL

Notes.

we do not include in the final results; and the number of global samples to 15,000. MCMC fittings are performed twice, one with For the main components, we calculate the peak energy (E the initial parameter values, and the other one with the resultant the $E^2dN dE$ spectrumFor the standard BB componentine median parameter values.

best-fitting modefor our sampling SGRBssuch as the Akaike Information Criterion (AIC; Akaike 1974) and the Bayesian Information Criterion (BICSchwarz 1978). Here we prefer the our MCMC fittings. Given any two estimated models, the preferred modes the one that provides the smaller BIC value. Here we use the difference in BIC value (\triangle BIC = \square \square \square (model B) to the best model (model A) in the model comparisons. 40 and 12 GER (Franging from ~-2.1 to −1.5, If \triangle BIC is larger than 10, the evidence agains the candidate model is very strong (Kass & Raftery 1995).

3. Results

3.1. Best-fitting Models

Comparison results of different models of 13 SGRBs are presented in Table 4. We identify three subclasses according the best-fit models: eight GRBs are best fitted by the BB+PL model (Class A), four GRBs by the CPL+PL model (Class B), and GRB 090510 by the BAND+PL model (Class C). The spectralenergy distributions (SEDs) for 3 GRBs from each subclass,namely GRB 081024B, GRB 090227B, and GRB 090510, are plotted together with the marginal posterior distributions in Figure 2, while the SEDs for the other 10 GRBs are shown in Appendix Figures B2 and B3. In all SEDs, we calculated the residual values $(f_y - f_m)^2/s_{f_d}^2$, where f_g sf, are the binned observationaffermi data and the corresponding 1σ errors and f_m are the fluxes calculated by the bestfitting models. All residuals in 13 GRBs are between 0 and 3.0, Pearson correlation coefficient (R1 < R < 1) is close to 1. which imply good spectrafittings for all GRBs. All resultant

Hereafter, we categorize the BB, BAND, and CPL functions $n = 0.80 \pm 0.31$. The best fit for the correlation is written as as the main component and the PL function as the extra PL component. The extra PL component is present in all 13 analyzed SGRBs, which might imply the common existence of where both F_{PL} and F_{main} are in units of erg cm² s⁻¹. This an extra energy dissipation process in SGRBs.

3.2. Parameter Distributions

median parameter values.

In order to know which of a suite of models best represents the tipe that is, \(\mathbb{F}_{B,B} \approx 3.92 \) k\(\mathbb{F}_{B} \), which is also employed in Zhang et al. best-fitting models our sampling SGRBs uch as the Akaike (2020) and Tak et a(2019). For the CPL components peak energy is calculated as $E_c = (2 + \alpha)E_c$. The values of the peak energy (F,BB Ep,CPL and Fp,BAND) are reported in Table As BIC for selecting a best-fitting model due to the large sampling in found thatthe peak energies of the main components of GRBs that are best-fitted with CPL or BAND are larger than those bestfitted with BB.

> For the extra component the observed spectra are generally e.g., 10 out of 13 GRBs in our sample with central values of Γ larger than -2.0. Note that it does not necessarily mean the absence of a softer PL component in reality, because GRBs with softer PL components may not be detectable to Fermi-LAT.

3.3. Correlation between Frain and FPL

Spectral fluxes between 8keV and E_{max} (the maximum photon energy detected by Fermi-LAT) are calculated by the terminate the terminate $\frac{1}{2}$ spectrum, denoted by $\frac{1}{2}$ spectrum, denoted by $\frac{1}{2}$ main component and FPL for the extra PL component. Then, we test the correlation between them by a linear fit in logarithm space such as

$$\log F_{\rm PL} = m + n \log F_{\rm main} \tag{7}$$

where m and n are the free parameters. This fitting is performed by the basic linear regression analysis in the populaOrigin scientific package, which can give the coefficient of determination (R^2 , 0 < R^2 < 1). For the linear fit, two variables, such as F_{main} and F_{PI} in our work, are positively correlated if the

We found a moderate correlation between Fand Fpl for parameters of the best-fitting models are presented in Table 5 all GRBs in our sample, with R = 0.62, m = -2.17 ± 1.67 , and

$$\log F_{\rm Pl} = 10^{2.171 \cdot 1.67} + (0.801 \cdot 0.31) \log F_{\rm main} \tag{8}$$

correlation is plotted in the left panel of Figure 4, in which two

^a Best-fitting model with \triangle BIC = 0.

b >10 represents the best model against this candidate model.

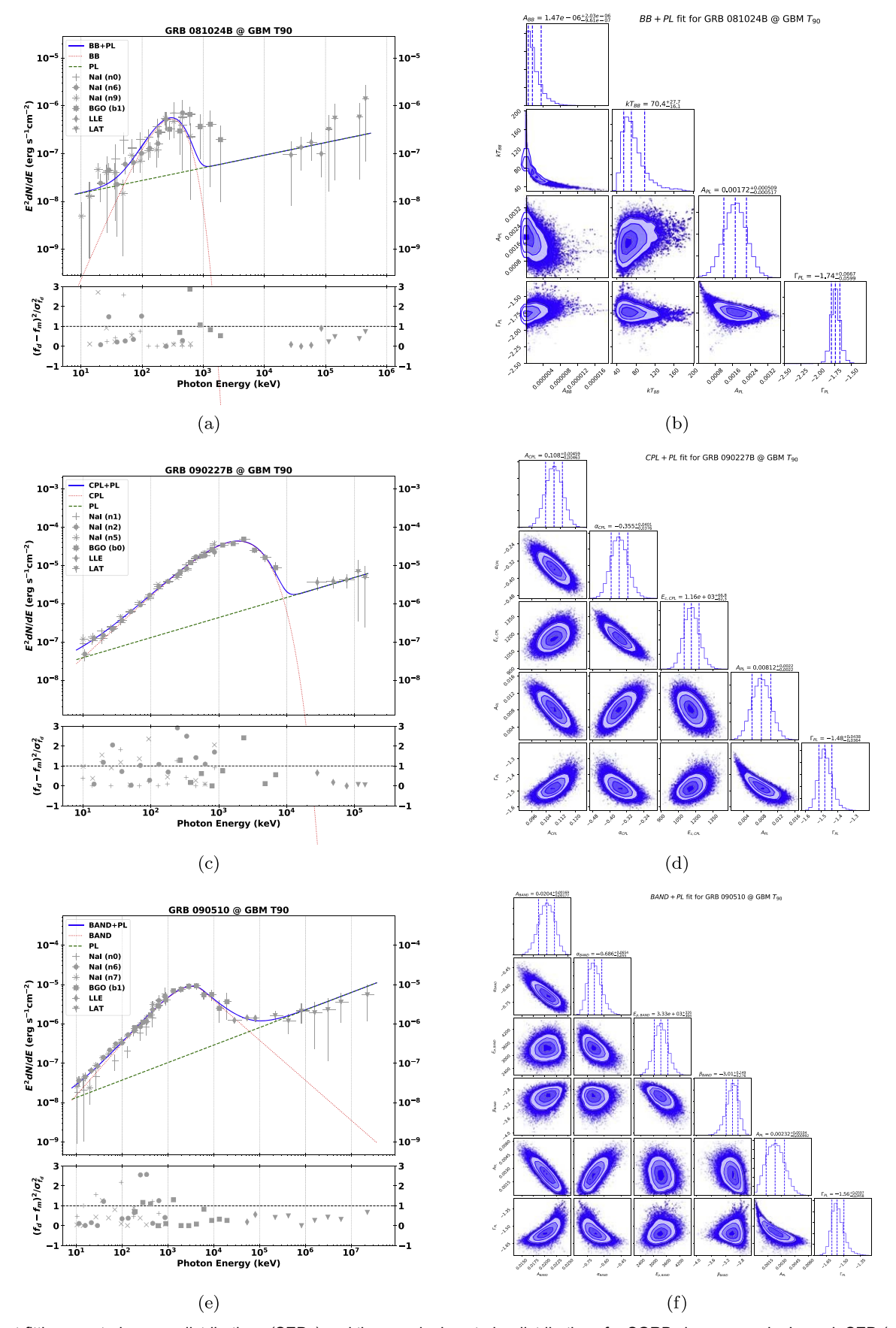


Figure 2. Best-fitting spectral energy distributions (SEDs) and the marginal posterior distributions for SGRBs in our sample. In each SED (a, c, e), gray points are to binned observational data by Fermi, the red dotted line is the modeled main component, the green dashed line is the modeled extra PL component, and the blue so line represents the sum of both components.

Table 5 Derived Parameters of the Best-fitting Model in the TP Scenario

Class	Main Component				Extra PL Component		
BB+PL	A _{BB} ^a		E _{p, BB} ^b	F _{BB} ^c	A _{PL} ^d	Γ _{PL}	F _{PL} e
081024B	19.9 ± 15.0		301 ± 86	7.2 ± 5.4	171.0 ± 51.3	-1.74 ± 0.06	9.1 ± 2.7
081102B	13.1 ± 4.5		297 ± 32	4.4 ± 1.5	161.0 ± 41.8	-1.85 ± 0.12	5.4 ± 1.4
110728A	23.6 ± 11.5		244 ± 40	3.7 ± 1.8	17.9 ± 17.7	-1.93 ± 0.42	0.4 ± 0.4
120915A	12.5 ± 4.5		347 ± 42	8.0 ± 2.9	9.9 ± 9.6	-1.89 ± 0.42	0.2 ± 0.2
140402A	3.8 ± 1.4		588 ± 79	20.0 ± 7.5	19.8 ± 18.7	-2.13 ± 0.52	0.3 ± 0.2
141113A	3.0 ± 1.6		539 ± 111	11.3 ± 5.9	58.7 ± 53.7	-1.87 ± 0.35	1.7 ± 1.6
171011C	23.8 ± 3.5		209 ± 46	69.7 ± 1.5	17.2 ± 14.8	-1.90 ± 0.46	0.4 ± 0.4
190515A	2.4 ± 0.6		679 ± 114	22.2 ± 5.9	49.8 ± 40.3	-1.83 ± 0.25	1.7 ± 1.4
CPL+PL	A _{CPL} ^a	α _{CPL}	E _{p, CPL} b	F _{CPL} °	A _{PL} ^d	Γ _{PL}	F _{PL} e
090227B	10.8 ± 0.5	-0.35 ± 0.04	1915 ± 106	886.0 ± 37.7	813.0 ± 220.0	-1.48 ± 0.04	106.0 ± 28.7
090228A	10.0 ± 0.4	-0.27 ± 0.09	767 ± 85	192.0 ± 8.7	438.0 ± 238.0	-2.06 ± 0.22	6.0 ± 3.3
120830A	2.0 ± 0.1	-0.16 ± 0.11	1005 ± 159	67.2 ± 4.1	23.8 ± 23.5	-2.02 ± 0.43	0.4 ± 0.4
160709A	2.6 ± 0.2	-0.13 ± 0.08	1784 ± 180	269.0 ± 23.1	380.0 ± 100.0	-1.66 ± 0.05	24.7 ± 6.5
BAND+PL	A _{BAND} ^a	α _{BAND} (β _{BAND})	E _{p,BAND} ^b	F _{BAND} ^c	A _{PL} ^d	Γ_{PL}	F _{PL} ^e
090510	2.0 ± 0.2	-0.68 ± 0.06 (-3.02 ± 0.16)	3322 ± 316	241.0 ± 20.9	235.0 ± 103.0	−1.56 ± 0.05	229.0 ± 101.0

Notes.

GRBs, GRB 081024B and 081102B, are far from the bestlinear fit is performed by excluding GRBs 081024B and 081102B.In this case,F_{main} and F_{PL} have a stronger positive correlation than that in Equation (8), with R = 0.80, $m = -0.50 \pm 1.55$, and $n = 1.15 \pm 0.29$, which is presented as

$$\log F_{\rm PL} = 10^{\circ} \, ^{0.501} \, ^{1.55} + (1.15 \, \mathbb{D} \, 0.29) \log F_{\rm main}, \tag{9}$$

shown in the right panel of Figure 4. In this strong positive correlationGRBs 081024B and 081102B deviate from the corr-Asano et al. 2009; Wang et al. 2018), and proton synchrotron PL component to the main component with respect to the ratioseptonic models including the SSC scenario (Corsi allalob; other GRBs. This requires an efficient conversion of the jet's kiDatione et al2011), the external IC scenar(Joma et al2011; energy to nonthermal particles in the prompt emission phase of the er al. 2012), and the synchrotronradiation scenario GRB or implies an important contribution from the early afterglowa 2010) have been invoked as well. In the latter case, it requires an early deceleration of the GRB jet Spenerally, the extra PL componen (including high-energy the interstellamedium, probably caused by a high initiabulk Lorentz factor Γ_0 for the jet given the deceleration timescale of $t_{\text{dec}} = 0.5 (n_{\text{ISM}}/1 \text{ cm}^{-3})^{1/3} (E_k/10^{50} \text{ erg})^{1/3} (C_0/1000)^{-8/3} \text{ s}$ (Mészáros & Rees 1994).

4. Possible Origin of the Extra PL Components

In order to explore the possible origins of the extra PL components we need to understand two main features this spectral component, namely, the spectral slope, which is foundalectrons (or the leptonic modellin either scenariothe highapproximately range between [-2.0, -1.5] (see the middle panel province produced will likely be absorbed by the of Figure 3) and the flux amplitude relative to the ftthe main spectral component (see the bottom panel of Figure 3). The originmpact. The secondary electron/positron pairs will be of the extra high-energy emission (especially above 100 MeV) generated and radiate a new generation of photons via the IC still under debate. The late-time and long-lasting high-energy gamma-ray emission from GRBs, such as 080916C, 090510, athet magnetic field. The new generation of photons will repeat 090902B, may arise from afterglow emission rathethan the

prompt emission (Kumar & Barniol Duran 2009; Ghisellini et al. fitting line compared with the other GRBs. Therefore, a similar 2010; Razzaque 2011). However, the high-energy emission in the early stage presents a rapid variability and a temporal correlation with the keV/MeV emission, implying an internal dissipation origin (Maxham et al. 2011; Tang et al. 2017). The origin of the extra high-energy emission hich is usually detected by Fermi-LAT in the brightest GRBs, has been explained via various highenergy processes, such as Comptonized thermal, self-synchrotron Compton (SSC) (Rees & Mészáros 1994; Asano & Inoue 2007), proton-induced cascade (Vietige 97; Dermer & Atoyan 2006;

elation at about the 3σ level, with an excessively high ratio of themission (Totani 1998). Except for the one-zone model, multizone

part) implies the presence of nonthermal relativistic particles accelerated during the prompt emission phase, which can arise when a multiplicative stochastic process (threataches lognormal in equilibrium) is truncated before equilibrium is achieved (Mitzenmacher2004; Reed & Jorgensen 2004; Fang et al. 2012), such as in Fermi-type acceleration processites we consider two possible one-zone scenarios: one is the product of hadronic interactions ofaccelerated protons (othe hadronic model), and the other is the IC radiation of accelerated

radiation from the main component as the GRB fireball is guite process in the radiation field and via the synchrotron process in the above process unless the energies of the newly generated

^a Normalizations for the main component‱_{BB} in units of 10⁻⁷ ph keV⁻¹ cm⁻² s⁻¹, and A_{DPL} and A_{BAND} in units of 10⁻² ph keV⁻¹ cm⁻² s⁻¹.

^b Peak energy of the E²dN/dE spectrum in units of keV.

^c Fluxes of the main components in units of 10 erg cm⁻² s⁻¹

^d Normalization for the extra component in units of ₹5ph keV¹ cm⁻² s⁻¹.

e Flux of the extra PL component in units of 10 erg cm⁻² s⁻¹.

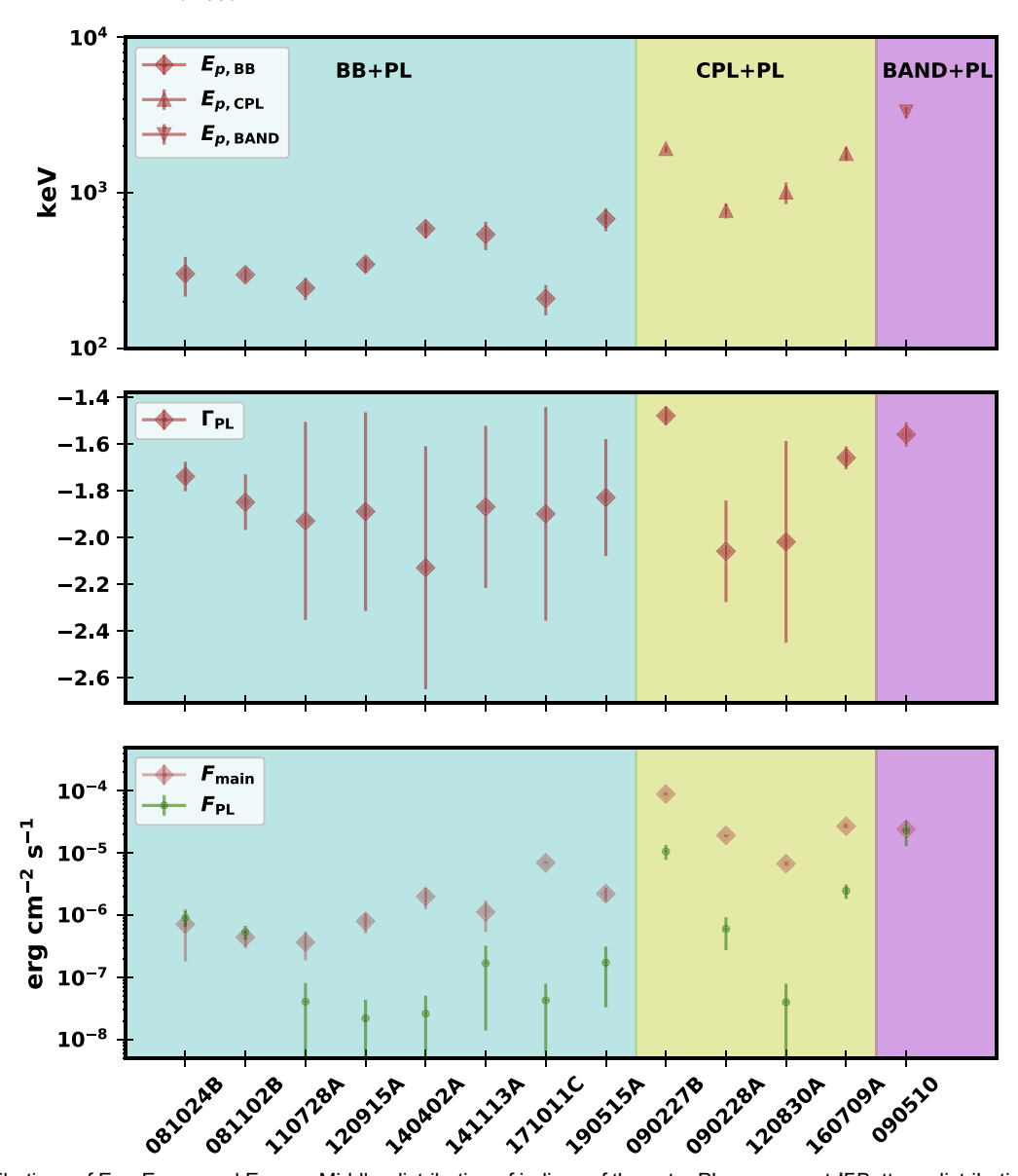


Figure 3. Top: distributions of E_{BB} , $E_{p,CPL}$ and $E_{p,BAND}$. Middle: distribution of indices of the extra PL component (E_{BB}) $E_{p,CPL}$ and $E_{P,BAND}$. Middle: distribution of indices of the extra PL component (E_{BB}) $E_{p,CPL}$ and the average flux of both components (E_{BB}). The cyan shading is for the class of BB+PL, the yellow shading is for the class of the CPL+PL, and the magenta shading is for the class of the BAND+PL.

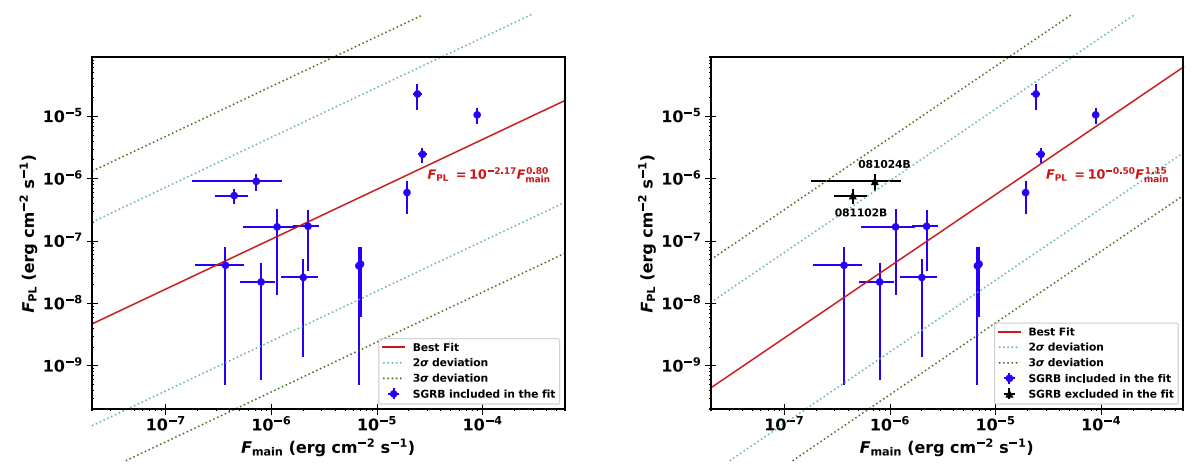


Figure 4. Left: linear fit for F_{main} and F_{PL} in the logarithm space for all GRBs in our sample. Right: linear fit F_{PL} in the logarithm space excluding GRB 081024B and GRB 081102BThe solid line is the best fit and the cyan and green dotted lines represent the 2σ and 3σ deviations from the best fit and the cyan and green dotted lines represent the 2σ and 3σ deviations from the best fit and the cyan and green dotted lines represent the 2σ and 3σ deviations from the best fit and the cyan and green dotted lines represent the 2σ and 3σ deviations from the best fit and the cyan and green dotted lines represent the 2σ and 3σ deviations from the best fit and the cyan and green dotted lines represent the 2σ and 2σ deviations from the best fit and the cyan and green dotted lines represent the 2σ and 2σ deviations from the best fit and 2σ deviations from the 2σ devia

photons drop below the threshold of the pair production process. Such a process is called the electromagnetic (EM) cascade It will largely modify the spectrum of the initially generated high-energy gamma-rays and dominate the PL component. To deal with the EM cascade processive follow the treatment described by Wang et al. (2018). Note that we do not aim to explain the main spectral component, so we simply treat it as a target photon field for vy annihilation and IC radiation. For the main spectra component although most of GRB prompt emission spectra around keV-MeV are present with a nonthermal shape and usually can be modeled as a smoothly broken power law, i.e., the BAND function, thermal emission originating from the photosphere is a natural prediction of the generic fireball scenario (Paczynskil 986; Shemi & Piran 1990; Mészáros et al.993; Pe'er etal. 2012; Hascoët et al. 2013). The relative strength of thermal emission and nonthermal emission should depend on the various environments(Daigne & Mochkovitch 2002; Ryde 2005). For the SGRB samples in this paper, the main spectral components of most of them can be described better by a BB emission. The detailed origin of the main spectral component is beyond the scope of this paper; here we only approximate it to be a BB emission in the calculation although in some GRBs the main spectral components are found to be best described with CPL or BAND.

We consider GRB located at z = 1 with a bulk Lorentz factor of $\Gamma = 300$ and a dissipation radius $R = 10^4$ cm. The main spectral component is assumed to be a diluted BB distribution with a temperature of kT = 100(1 + z) keV and an isotropic-equivalent luminosity of $_{BB} = 6 \times 10^{52}$ erg \bar{s}^1 .

For the hadronic model, the radiation at GeV energies is dominated by the EM cascade initiated by the hadronic processes including the photomeson (PM) processand the Bethe-Heitler (BH) process Protons can be accelerated at the dissipation radius by some processesg., internal shocks or magnetic reconnections n this case, we define a magnetic equipartition coefficient (a) as the ratio of the magnetic field energy density U₃ to the photon energy density of the BB componentU_{bb}, i.e., $\epsilon_B = U_B/U_{bb}$. The proton spectrum is assumed to be a PL distribution with a slope of p = -2 and a maximum proton energy $E_{p,\text{max}} > 0.15 \text{ GeV} \hat{G}^2/kT$ » 10^{17} eV in order to have an efficient photomeson process. The isotropi equivalent luminosity for protons is taken to be 6 x 10^{53} erg \bar{s}^1 , corresponding to a baryon loading factor of 10. The accelerated protons can generate high-energy gamma-ray hile fixing $\epsilon_B \neq 0.01$, the flux of synchrotron radiations of and electronsthrough the PM and BH processes and then initiate the EM cascade in the photon field and the magnetic field. As shown in Wang et al. (2018), different values of ε_B can lead to differentindexes of cascade emissiodue to the different ratios between the contributions from the synchrotron spectra become harder with a larger hoton index. radiation and that of the IC radiation. Indeed, as we can see in the top panel of Figure 5 for a larger $\varepsilon_{\rm B}$, the photon index is

For the leptonic modelsome electrons in the GRB fireball, in addition to those responsible for the main spectral temperatures and background photon teld distributions, the component, are assumed to be accelerated up to ultrarelativistic same electron PL distribution $dN_{i}dE = AE^{C_{i}}$ (the detailed energies with a PL distribution $dN_{i}dE = AE^{G}$. The IC

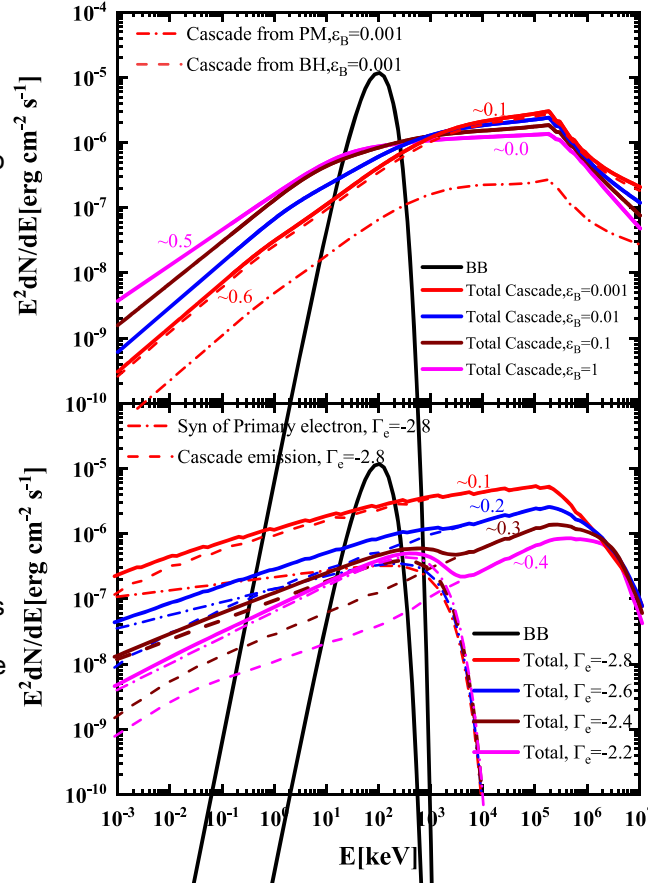


Figure 5. The extra components for the hadronic model (top) and leptonic model (bottom). In the bottom panel, the solid lines are the sum of the cascade emission (dashed lines) and the synchrotron adiation (dashed-dotted lines) primary electrons The approximate slopes for different lines are presented in diation (dashed-dotted lines) of the same colors.

scattering on both the BB component and the synchrotron radiation of these ultrarelativistic electrons themselves can give rise to high-energy radiation. Similar to that in the hadronic model, the high-energy radiation produced will trigger an EM cascade. The relative contribution from the synchrotron process and the IC process of the cascade emission depends on the lequipartition coefficients_B in the same way show in the hadronic scenarioso here we mainly explore the influence of the injection spectral index in the bottom panel of Figure 5 primary electron at 100 keV and the maximum electron Lorentz factor ∉mitting a typical photon energy of~1 MeV. For $\Gamma_e = -2.8$, the spectral shape of the extra component is a quite flat PL with photon index ~-1.9, and for a larger, The

We have also checked the dependence of our results on the assumed modeparameterse.g., the temperature of the BB, close to -2.0, while for a smaller_Bs the photon index tends to be larger. The photon index of the cascade emission in the 1–10 keV energy range is about -1.5 in all the cases because if the BAND function distribution with the typical values of the is mainly produced by the electrons cooled from higher energies and hence an E^{-2} spectrum is expected for these cooled electrons (Wang et al018).

So the length of rigidite 3,01 and a passion of the photon index in Figure 3 and a background photon field with the BAND function distribution with the typical values of the low-energy photon index $\alpha = -1.0$, the high-energy photon index $\beta = -2.2$, the peak energy $\beta = 1.0$ keV, and the peak flux of 10^{-5} erg cm² s⁻¹, is adopted to replace the different distribution. To explore the dependenceon the different origin of the BAND component is beyond the scope of the

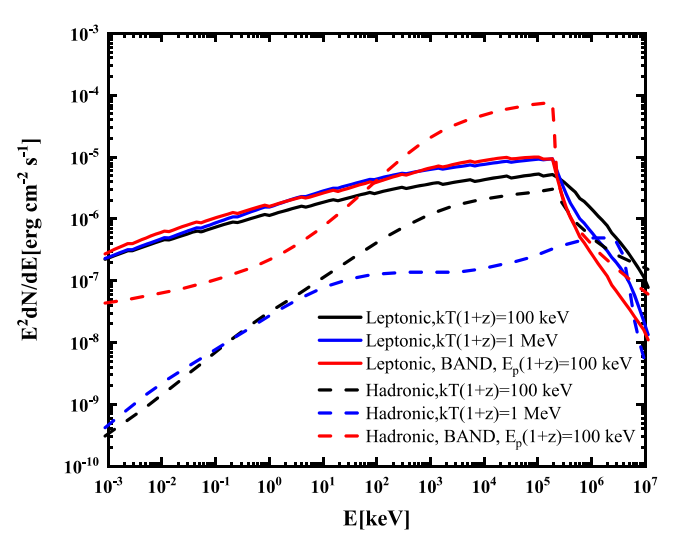


Figure 6. The effects for different background photon distributions. The hadronic model (solid lines) and the leptonic model (dashed lines) are shown with two temperatures (black and blue) for the BB background photon distribution and a BAND function (red) background photon distribution for the different temperatures of the BB component peak flux has the same value of 10^{-5} erg cm 2 s $^{-1}$. The parametersof the BAND component are α = -1.0, α = -2.2, and the same flux of 10^{-5} erg cm 2 s $^{-1}$ as the BB component. \grave{o}_B = 0.01 and Γ $_e$ = -2.8 are adopted for all lines. The other parameters are the same as the red lines in Figure 5 for the hadronic model a the leptonic model respectively (see text for details).

paper) and $\Gamma_e = -2.8$ are assumed for simplicity for the leptonic model, the same proton distribution as in Figure 5 is assumed forthe hadronic model, and the same $\dot{\phi}_i = 0.01$ is energy photon field including the initialphoton field (BB or BAND distribution) and the cascade emission in the keV to MeVonstrained by the stacking observation becube as it was fully developed due to the relatively high photon densitAs shown in Figure 6, for the leptonic model, different temperatures (black and blue solid lines) would produce similarradiations because the EM cascade is fully developed and the low-energy In this paper, we looked into the extra PL spectral photons from keV to MeV energies are approximately dominated photons from keV to MeV energies are approximately dominated photons from keV to MeV energies are approximately dominated photons from keV to MeV energies are approximately dominated photons from keV to MeV energies are approximately dominated photons from keV to MeV energies are approximately dominated photons from keV to MeV energies are approximately dominated photons from keV to MeV energies are approximately dominated photons from keV to MeV energies are approximately dominated photons from keV to MeV energies are approximately dominated photons from keV to MeV energies are approximately dominated photons from keV to MeV energies are approximately dominated photons from the keV to MeV energies are approximately dominated photons from the keV to MeV energies are approximately dominated photons from the keV to MeV energies are approximately dominated photons from the keV energies are approximated photons from the keV energies are approximated photon from the keV energies are approximated photons from the keV energies and the keV energies are approximated photons from the keV energies and the keV energies are approximated photons from the keV energies are approximated photon from the keV energies are approximated photons from the keV energies are approximated photon from the keV energies are approximated pho by the high-flux cascademission. For the BAND function shows a similar spectral shape and the magnitude of the cascade B 160709A, whose extra PL component was already flux depends principally on the background photon field and the previously reported in the literature. The average flux of the adopted electron distribution. For the hadronic model in Figure \mathbb{BL} components within the \mathcal{J}_0 scale positively correlates with because the low-energy photons anging from keV to MeV energies from the cascade emission is weaker than those from Phecomponents of short GRBs are distributed in the range initial BB component the initial BB component with the same peak flux and a higher temperature provides lower photon density, inducing lower cascade emission. When a BAND function relectrons accelerated in the prompt mission phaseln the distribution is involved in the hadronic modelhigher cascade flux is expected becauseve fixed the flux of the BAND component to be 10 erg cm2 s-1, the same as that the BB component and the low-energy photon index of the BAND component, -1.0, is much smaller than that of the BB component termining which is the preferred one of these two models. so that the BAND component provides much more photons with

luminosity for the cascade emissio At the eV to keV energy

as the radiation below keV is mainly produced through the

annihilation ratherthan by the electronscooled from higher energies (the latter one usually shows a typical fast cooling photon index, i.e., ~-1.5). The BAND function distribution provides much more target photons with energies belown increases the photon-photon annihilation opacity. Except for the flattening at the eV-keV energy range for the BAND function in the hadronic model, the other characteristics of the spectral shapes for either the hadronic model or leptonic model at different temperatures of the BB componentor even treating the background photon field as a BAND function do not change significantly compared with those in Figurer 5 addition, even when taking such flattening thate eV to keV energy range into account, the spectra for a quite large energy range extending from eV to GeV could be treated approximately as a PL component.

In summary, as shown in Figure 5, both models can produce an approximate PL componentinging from keV to GeV energies within a certain range of indices, which is consistent with our result of extra PL componenfor the SGRBsHowever, for a flat PL component with a photon index close to -2.0 the low-energy excess up to 10 keV could be helpftol tell us which models preferred because for the former one the photon index of the lowenergy excess close to -1.5 while for the latter one it is $\sim (\Gamma_e - 1)/2$. Nevertheless, the poor statistics at a few keV makes it difficult to differentiate the two models with current observations. On the other hand, the cascade emissions both models can extend down to the optical band, as shown in Figure 5, and the flux difference athe opticalband between the two models becomes distinct. Therefore, in the future, observations in the optical band of the prompt emission of GRBs may tell us which model is preferable. In addition, the hadronic model usually needs to invoke a relatively larger kinetic luminosity than the leptonic model due to

adopted for both models. The final cascade emission depends thre lower radiation efficiency of protons than electrons and maybe whether the EM cascade is fully developed and on the total lowexceed the typical energy budgets of GRBs. The hadronic model also naturally predicts neutrino production, which might be energy range. In the GRB environment, the EM cascade is likelyone in the case of LGRBs (Aartsen et al. 2015, 2016, 2017).

5. Summary and Conclusion

Fermi-GBM and LAT data, we identified the PL component distribution as the background photon filed, the cascade emissionall 13 short GRBs in our sample, including GRB 090510 and that of the main spectrabomponents. The slopes of the extra between -2.0 to -1.5, which may be well reproduced by considering the EM cascade induced by ultrarelativistic protons future, observations with more statistics around the keV energy band and observations of the prompt optical GRB emission may tell us which model is preferable. In addition, the nextgeneration neutrino telescopesmight play a key role in

energies below, than the BB component and makes the hadronic We thank the anonymous reference ho helped improve the processes (PM and BH) more efficient, inducing a higher injectionanuscript, and the statistics editor for helpful suggestions. We are grateful to Yu Wang and Donggeun Tak for range, the radiation becomes flat (the red dashed line in Figured®)cussions. This research madeuse of the High Energy Astrophysics Science Archive Research Cent(et EASARC) synchrotron radiation process by electrons from photon-photonOnline Service at the NASA/Goddard Space Flight Center

(GSFC). This work is supported by the NSFC under grants 11903017,12065017,12003007,U2031105, and 11975116, and the Fundamental Research Funds for the Central Universities (No.2020kfyXJJS039).

Facilities: Fermi-GBM, Fermi-LAT.

Software: Origin 7.0 hosted by OriginLab Corporation, 3ML (Vianello et al. 2015).

Appendix A

Comparisons of Results between the Uniform Priors (UP) Scenario and the Typical Priors (TP) Scenario

In this section, we test the uniform-distribution priors for all parameters of six models, hereafternamed UP. In the UP

scenario,all normalizations (A)photon indices $(\alpha,\beta,$ and $\Gamma)$, and parameters of the break energy (kT, E_c and E_p) are distributed uniformly, employing the same range as that in the typical priors (TP) scenario.

The best-fitting models are shown in Table A1. Of 13 GRBs with Δ BIC equals 0 (Best Model), 10 GRBs prefer the one-componentmodel and 3 GRBs the two-componentmodel. There are several andidate models with Δ BIC less than 10, which cannotbe rejected by the best-model-selection method described in Section 2.4.2Therefore,in the UP scenario,we divided the best-fitting models into the best-fitting one-componentmodels (Best1C Model) and the best-fitting two-component models (Best 2C Model).

Table A1 ΔBIC and the Best-fitting Models in the UP Scenario

GRB	BB	Band	CPL	BB+PL	BAND+PL	CPL+PL	Best Modef	Best 1C Mode	Best 2C Mode
081024B	>10 ^d	0	7	5	>10	7	BAND	BAND	BB+PL
081102B	>10	6	0	6	>10	>10	CPL	CPL	BB+PL
090227B	>10	>10	>10	>10	7	0	CPL+PL	L	CPL+PL
090228A	>10	7	2	>10	5	0	CPL+PL	CPL	CPL+PL
090510	>10	6	>10	>10	0	>10	BAND+PL	BAND	BAND+PL
110728A	0	>10	6	8	>10	>10	BB	BB	BB+PL
120830A	>10	6	0	>10	>10	8	CPL	CPL	CPL+PL
120915A	0	>10	4	9	>10	>10	BB	BB	BB+PL
140402A	0	>10	6	7	>10	>10	BB	BB	BB+PL
141113A	0	7	1	9	>10	>10	BB	BB	BB+PL
160709A	>10	0	>10	>10	2	1	BAND	BAND	CPL+PL
171011C	0	>10	4	8	>10	>10	BB	BB	BB+PL
190515A	1	6	0	9	>10	>10	CPL	CPL	BB+PL

Notes.

Table A2
Derived Parameter Values of the Best 2C Model in the UP Scenario

Class	Main Component			Extra PL component	
BB+PL	A _{BB} ^a		E _{p,BB} ^b	A _{PL} °	Γ _{PL}
081024B	21.8 ± 15.9	L	297 ± 85	175.0 ± 50.1	-1.74 ± 0.06
081102B	13.3 ± 4.6	L	295 ± 32	162.0 ± 42.3	-1.85 ± 0.12
110728A	21.9 ± 16.8	L	231 ± 42	37.7 ± 30.8	-1.91 ± 0.38
120915A	12.7 ± 4.7	L	346 ± 43	17.7 ± 16.3	-1.85 ± 0.37
140402A	3.8 ± 1.4	L	586 ± 75	29.4 ± 25.8	-2.21 ± 0.61
141113A	3.0 ± 1.7	L	535 ± 116	76.8 ± 58.7	-1.85 ± 0.32
171011C	30.4 ± 17.1	L	212 ± 43	19.9 ± 17.9	-1.89 ± 0.43
190515A	2.4 ± 0.6	L	674 ± 110	57.3 ± 39.8	-1.85 ± 0.24
CPL+PL	A _{CPL} ^a	α _{CPL}	E _{p,CPL} ^b	A _{PL} ^c	 Γ _{PL}
090227B	10.8 ± 0.5	-0.35 ± 0.04	1915 ± 106	824.0 ± 214.0	-1.48 ± 0.04
090228A	9.6 ± 0.4	-0.34 ± 0.09	767 ± 79	452.0 ± 221.0	-2.02 ± 0.20
120830A	1.9 ± 0.1	-0.14 ± 0.11	1000 ± 155	36.7 ± 32.6	-2.01 ± 0.40
160709A	2.6 ± 0.2	-0.14 ± 0.08	1794 ± 182	386.0 ± 95.5	-1.66 ± 0.05
BAND+PL	A _{BAND} ^a	α _{BAND} (β _{BAND})	E _{p,BAND} ^b	A _{PL} ^c	Γ_{PL}
090510	2.0 ± 0.2	-0.68 ± 0.06 (-3.04 ± 0.17)	3348 ± 318	252.0 ± 98.9	-1.56 ± 0.05

Notes.

^a Best-fitting model with Δ BIC = 0.

^b Best-fitting model with the lowest ΔBIC among the BBAND, and CPL models.

^c Best-fitting model with the lowest ΔBIC among the BB+PLBAND+PL, and CPL+PL models.

^d >10 represents the best model against this candidate model.

a Normalization for the main component A_{BB} in units of 10^{-7} ph keV⁻¹ cm⁻² s⁻¹, and A_{CPL} and A_{BAND} in units of 10^{-2} ph keV⁻¹ cm⁻² s⁻¹.

b Peak energy of the 2dN dE spectrum in units of keV.

^c Normalization for the extra components in units of 70ph keV¹ cm⁻² s⁻¹.

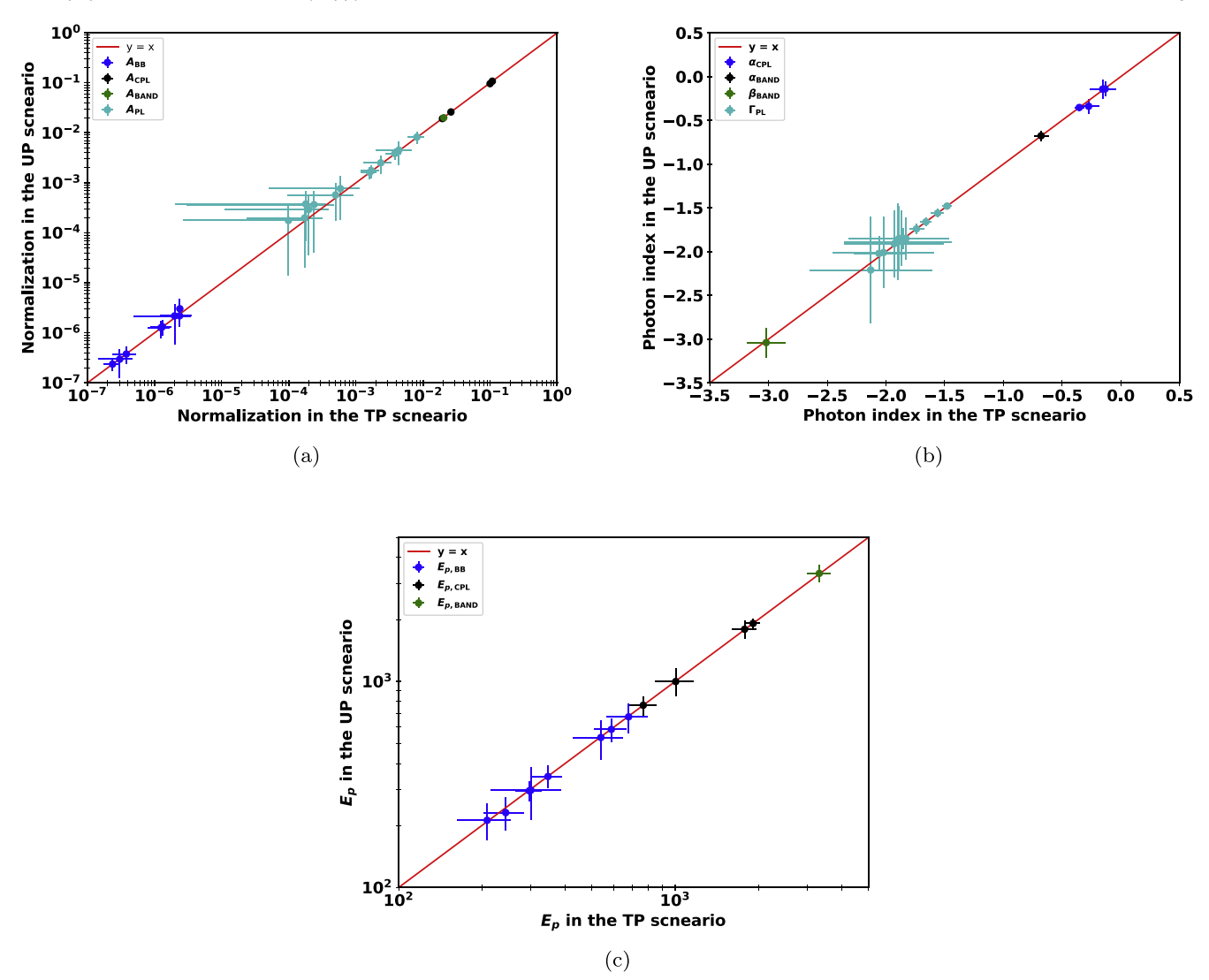


Figure A1. Derived parameters compared between the TP and UP scen $\overline{\textbf{X}}$ fiested solid line indicates y = x.

In order to compare results in the UP scenario with those in the TP scenario, we thus selected the Best 2C model. As showscenario are consistentith that of the bestmodels in the TP in Table A1, the Best 2C model of each GRB in the UP scenario is the same as the beshodel of the corresponding GRB in the TP scenario. The resultant parameters in the Best 2C model are reported in Table A2.

After all parameters are available in both the UP scenario and the TP scenario, we thus plotted the correlations of the same parametersin two scenarios, which are shown in Figure A1. The parameters of the photon indices, the peak energies and the normalizations in both scenariase almost lying at the equality (y = x) line.

In summary, the results of the best 2C models in the UP scenario. Therefore, only the results in the TP scenario are presented in the main text.

Appendix B Spectral Energy Distributions with the Best-fitting Model for the Other 10 SGRBs

In this section, we plot the spectral energy distributions with the best-fitting model for the other 10 SGRBs in Figure B2 and Figure B3.

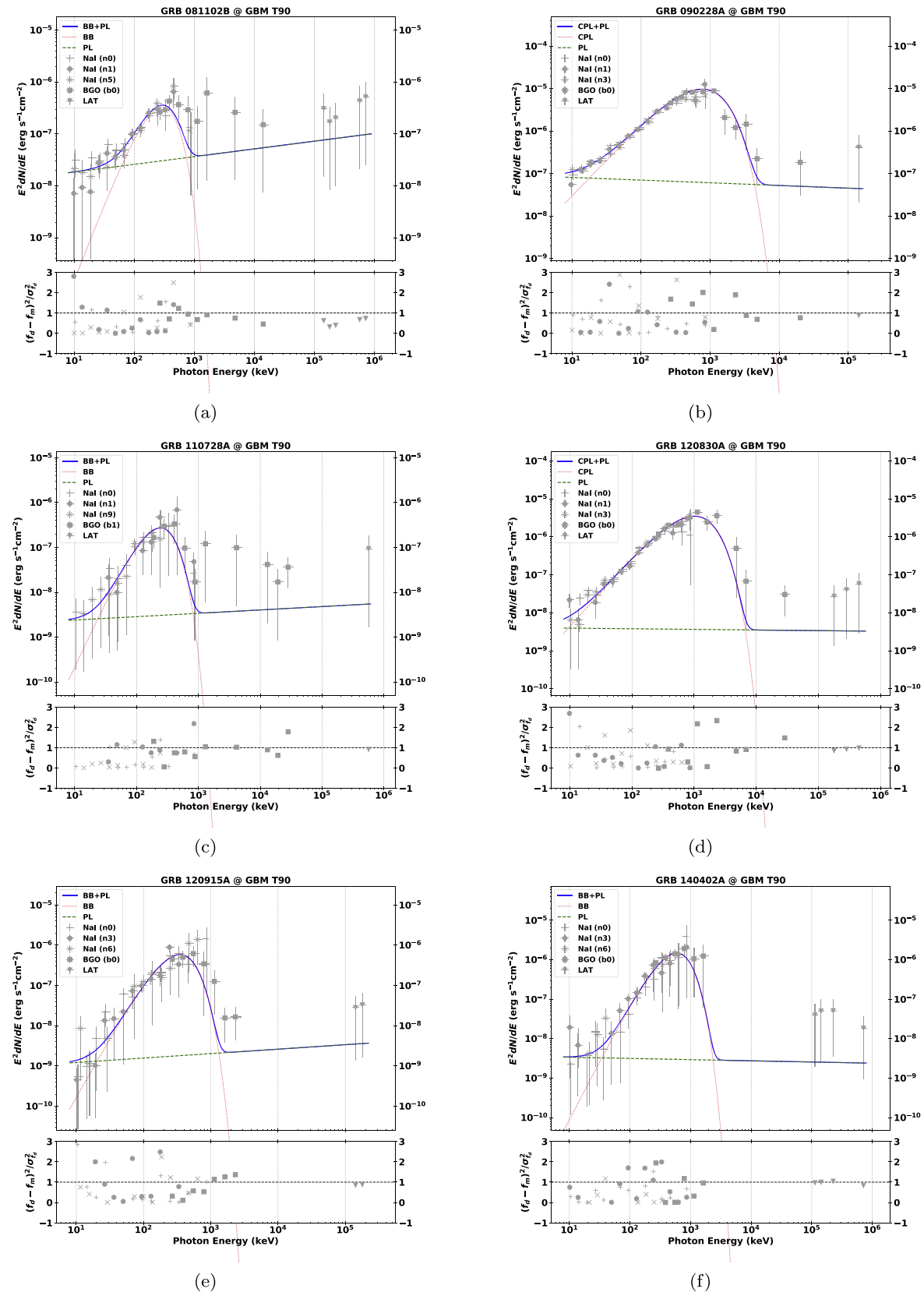


Figure B2. Same as the SEDs in Figure 19 tfor GRBs (a) 081102B(b) 090228A,(c) 110728A,(d) 120830A,(e) 120915A,and (f) 140402A.

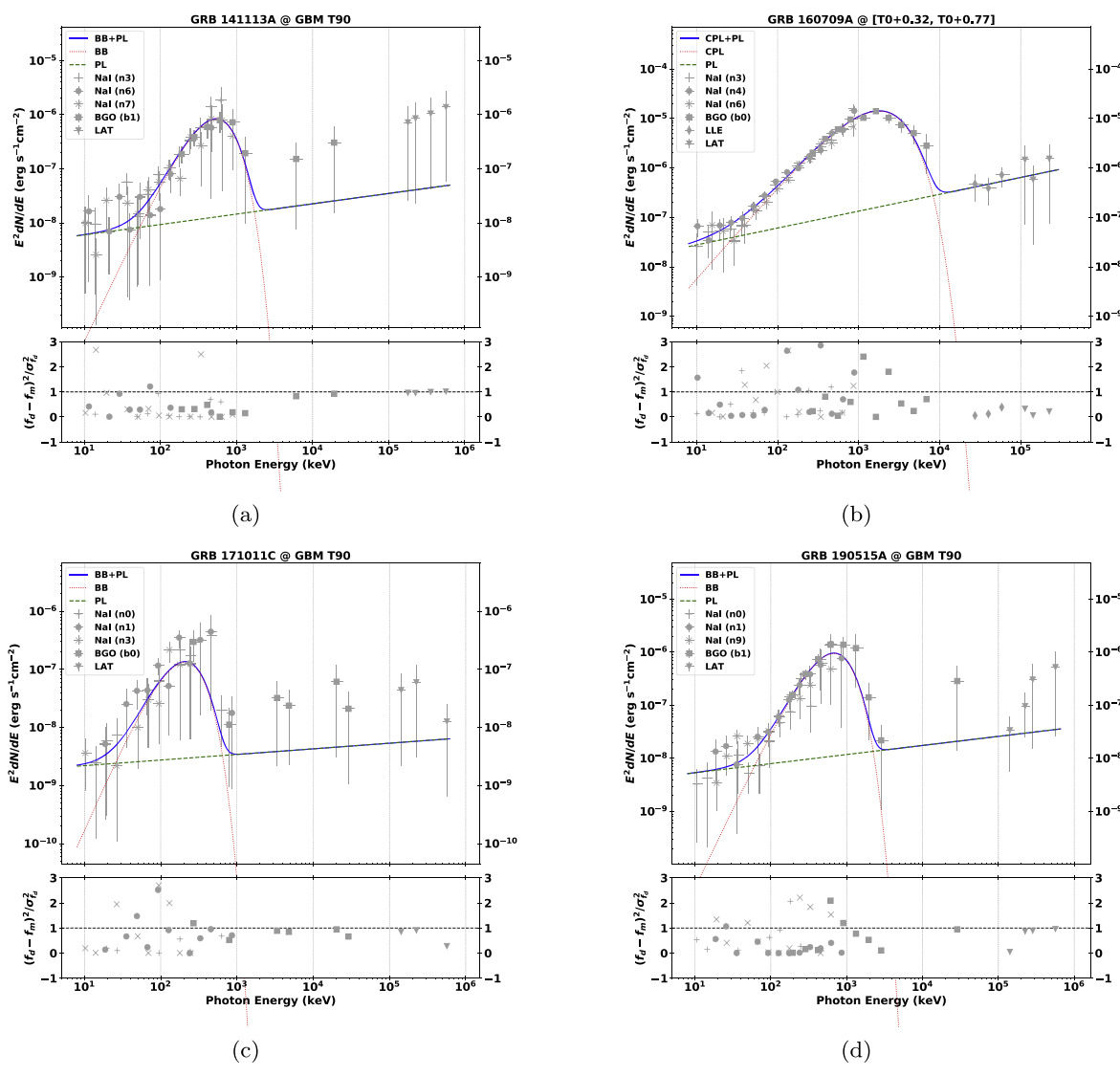


Figure B3. Same as the SEDs in Figure but for (a) GRBs 141113A(b) 160709A,(c) 171011C,and (d) 190515A.

ORCID iDs

Qing-Wen Tang® https://orcid.org/0000-0001-7471-8451 Liang Li ® https://orcid.org/0000-0002-1343-3089 Ruo-Yu Liu ® https://orcid.org/0000-0003-1576-0961

References

Aartsen, M., Abraham, K., Ackermann, M., et al. 2016, ApJ, 824, 115 Aartsen, M., Ackermann, M., Adams, J., et al. 2015, ApJL, 805, L5 Aartsen, M. G., Ackermann, M., Adams, J., et al. 2017, ApJ, 843, 112 Ackermann, M., Ajello, M., Asano, K., et al. 2013, ApJS, 209, 11 Ackermann, M., Asano, K., Atwood, W. B., et al. 2010, ApJ, 716, 1178 Ajello, M., Arimoto, M., Axelsson, M., et al. 2019, ApJ, 878, 52 Akaike, H. 1974, ITAC, 19, 716 Arimoto, M., Asano,K., Tachibana,Y., et al. 2020, ApJ, 891, 106 Asano, K., & Inoue, S. 2007, ApJ, 655, 762 Asano, K., Guiriec, S., & Mészáros, P. 2009, ApJL, 705, L191 Asano, K., & Mészáros, P. 2011, ApJ, 739, 103 Band, D., Matteson, J., Ford, L., et al. 1993, ApJ, 413, 281 Basak,R., & Rao, A. R. 2013,ApJ, 768, 187 Beloborodov,A. M. 2011,ApJ, 737,68 Beloborodov, A. M., Hascoët, R., & Vurm, I. 2014, ApJ, 788, 36 Bošnjak,Ž., Daigne,F., & Dubus, G. 2009, A&A, 498, 677 Corsi, A., Guetta, D., & Piro, L. 2010a, A&A, 524, A92 Corsi, A., Guetta, D., & Piro, L. 2010b, ApJ, 720, 1008

Daigne, F., Bosnjak, Z., & Dubus, G. 2011, A&A, 526, 110 Daigne, F., & Mochkovitch, R. 1998, MNRAS, 296, 275 Daigne, F., & Mochkovitch, R. 2002, MNRAS, 336, 1271 Dermer, C. D., & Atoyan, A. 2006, NJPh, 8, 122 Fang, Z., Wang, J., Liu, B.-Y., & Gong, W.-B. 2012, Handbook of Optimization in Complex Networks (Berlin: Springer), 55 Fraija, N., Lee, W. H., Araya, M., et al. 2017, ApJ, 848, 94 Giannios, D., & Spruit, H. C. 2007, A&A, 469, 1 Ghisellini, G., Ghirlanda, G., Nava, L., & Celotti, A. 2010, MNRAS, 403, 926 Goodman, J., & Weare, J. 2010, ApMaC, 5, 65 Hascoët,R., Daigne,F., & Mochkovitch, R. 2013, A&A, 551, A124 loka, K. 2010, PTEP, 124, 667 Iyyani, S., Ryde, F., Ahlgren, B., et al. 2015, MNRAS, 450, 1651 Kass, R., & Raftery, A. 1995, J Am Stat Assoc, 90, 773 Kawakubo, Y., Sakamoto, T., Nakahira, S., et al. 2018, PASJ, 70, 6 Kocevski, D., Axelsson, M., Scotton, L., et al. 2019, GCN, 24560, 1 Kobayashi, S., Piran, T., & Sari, R. 1997, ApJ, 490, 92 Kumar, P., & Barniol Duran, R. 2009, MNRAS, 400, L75 Li, L. 2019, Ap Li, L., Ryde, F., Pe'er, A., et al. 2021, ApJS, 254, 35 Maxham, A., Zhang, B.-B., & Zhang, B. 2011, MNRAS, 415, 77 MészárosP., Laguna,P., & Rees,M. J. 1993,ApJ, 415, 181 MészárosP., & Rees,M. J. 1994,MNRAS, 269,L41 Mitzenmacher M. 2004, Internet Math., 1, 2 Narayana Bhat, P., Meegan, C. A., von Kienlin, A., et al. 2016, ApJS, 223, 28 Paczynski, B. 1986, ApJ, 308, L43 Pe'er, A. 2008, ApJ, 682, 463

```
Pe'er, A., Zhang, B.-B., Ryde, F., et al. 2012, MNRAS, 420, 468
Poolakkil, S., PreeceR., Fletcher, C., et al. 2021, ApJ, 913, 60
Razzaque S. 2011, ApJ, 724, L109
Reed, W. J., & Jorgensen M. 2004, Commun. Stat, 33, 8
Rees, M. J., & Mészáros, P. 1994, ApJ, 430, L93
Rees, M. J., & Mészáros, P. 2005, ApJ, 628, 847
Ryde, F. 2005, ApJ, 625, L95
Ryde, F., Axelsson, M., Zhang, B. B., et al. 2010, ApJL, 709, L172
Schwarz, G. 1978, AnSta, 6, 461
Shemi, A., & Piran, T. 1990, ApJ, 365, L55
Spruit, H. C., Daigne, F., & Drenkhahn, G. 2001, A&A, 369, 694
```

```
Tak, D., Guiriec, S., Uhm, Z. L., et al. 2019, ApJ, 876, 76
Tang, Q.-W., Wang, X.-Y., & Liu, R.-Y. 2017, ApJ, 844, 56
Toma, K., Wu, X. F., & Mészáros, P. 2011, MNRAS, 415, 1663
Totani, T. 1998, ApJ, 509, L81
Vietri, M. 1997, PhRvL, 78, 4328
Vianello, G., Lauer, R. J., Younk, P., et al. 2015, arXiv:1507.08343
von Kienlin, A., Meegan, C. A., Paciesas W. S., et al. 2014, ApJS, 211, 13
Wang, K., Liu, R.-Y., Dai, Z.-G., & Asano, K. 2018, ApJ, 857, 24
Yu, H.-F., Dereli-Bégué H., & Ryde, F. 2019, ApJ, 886, 20
Zhang, B., & Yan, H. 2011, ApJ, 726, 90
Zhang, Z. B., Jiang, M., Zhang, Y., et al. 2020, ApJ, 902, 40
```